Theoretical and Applied Fracture Mechanics 137 (2025) 104864

Contents lists available at ScienceDirect

Theoretical and Applied Fracture Mechanics

journal homepage: www.elsevier.com/locate/tafmec

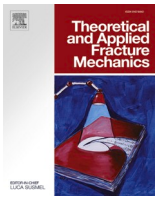

Experimental and numerical investigations on the synergistic effect of plasma nitriding and notch size on the fatigue properties of AISI 4140 steel

F. Yılan [a,*], H. Kovacı [b]

[a] Kırşehir Ahi Evran University Faculty of Engineering-Architecture Department of Mechanical Engineering Kırşehir Turkey
[b] Ataturk University Faculty of Engineering Department of Mechanical Engineering Erzurum Turkey

ARTICLE INFO

Keywords:
Notch fatigue strength
Stress intensity factor
Plasma nitriding
AISI 4140 steel
Finite element analysis

ABSTRACT

Engineering structures across various sectors frequently experience fatigue damage under operational conditions, which significantly reduces their operational lifespan. Moreover, fatigue strength of the materials reduces when they have geometries such as notches and sharp corners because they constitute stress concentrations. On the other hand, different surface treatments can efficiently increase in managing the lifetime and performance of materials. In the current study, the fatigue properties of untreated and plasma nitrided notched steel samples were compared through numerical analyses and fatigue experiments. For this investigation, fatigue test specimens with different notch sizes made out of AISI 4140 steel were plasma nitrided at 460 °C and 535 °C for 9 h in a glow discharge environment. The specimens were analysed using XRD, SEM, and microhardness tester to ascertain their structural, morphological, and mechanical characterization. The notch fatigue behaviour of nitride samples was analysed numerically by the Finite Element Analysis (FEA). Furthermore, a rotational bending fatigue test system was utilized to conduct fatigue tests and consequently, fatigue date obtained from experimental results and FEA were compared. It was found that the thicknesses of compound layer and diffusion zone, compressive residual stresses, and hardness enhanced as the process temperature increased. Additionally, an increase of by up to 110 % was obtained in the notch fatigue resistance of the specimens under constant amplitude loading. According to the results obtained, it was observed that there were acceptable errors between the experimentally obtained values and the values obtained from the FEA. The results show that in all plasma nitrided notched samples, the fatigue crack initiation shifted towards the core and thus the fatigue strength increased, and especially at the increasing plasma nitriding process temperature, the R4 and R8 notch geometries exhibited better fatigue performance improvement than the other samples.

1. Introduction

AISI 4140 steel are placed in numerous areas such as automotive, aerospace and defence industries because it is resistant to high pressure and impact [1–3]. However, surface or exterior layers of this material subjected to significant damages including wear, corrosion fatigue and fracture [4]. From this point of view, the various types of notches found in mechanical components, including steps, holes, and keyways, play a crucial role in determining the extent of fatigue damage, a primary mechanism of mechanical failure. Researches demonstrates that notches can induce stress concentrations within mechanical components. When these components are exposed to cyclic loading, the notches often become the initiation sites for failure. The surface condition of the material directly determines fatigue damage, which is one of the major mechanical damage mechanisms [5]. Therefore, there is a need to enhance the surface characteristics of material. As a thermochemical surface treatment, plasma nitriding (PN) a treatment known to improve the fatigue resistance of the materials by forming hard surface layers, increasing surface hardness and constituting compressive residual stresses [6–10].

As previously proposed, the fatigue characteristics of plasma nitrided on metallic materials have been investigated in various independent studies. In this regard, Şirin et al. [11] examined how the fatigue strength of AISI 4340 steel is influenced by the temperature at which plasma nitriding occurs. According to their statement, the fatigue strength exhibited a positive correlation with the rise in plasma nitriding temperature from 500 °C to 540 °C. Mohammadzadeh et al. [12] carried out experiments on various gas mixtures at 450 °C temperature for 8 h to

* Corresponding author.
E-mail address: faik.yilan@ahievran.edu.tr (F. Yılan).

https://doi.org/10.1016/j.tafmec.2025.104864
Received 30 November 2024; Received in revised form 7 January 2025; Accepted 3 February 2025
Available online 7 February 2025

see the gas mixture's effect on microstructure and wear properties in the AISI M2 tool. They found that the nitride layer thickness increased when the nitrogen ratio in the gas mixture increased after the plasma nitriding process. Kovacı et al. [13] inhibited the development of fatigue cracks by enhancing the surface hardness and inducing compressive residual stress using plasma nitriding treatment on AISI 4140 steel.

As examined earlier, the PN process has a substantial influence on the experimental investigation across all levels of different process parameters, including temperature, gas mixture and process time. However, the experimental study being carried out with a limited number of plasma nitriding conditions, mainly because fatigue test is time-consuming. Many variables and their variations can be studied using theoretical approach such as the FEA to examine the influence of plasma nitriding conditions on notch parts [14–19]. FEA is a numerical solution method that seeks solutions to various engineering problems with acceptable precision. Nowadays, more effective and faster results are obtained by using the FEA in optimizing performance of materials and examining factors such as fatigue behaviour, safety factor, stress distribution, deformations and forces [20–22]. However, only a few studies were performed to support the fatigue analysis of numerical results obtained from plasma nitrided materials via the finite element method. Yildiz et al. [23] utilized the finite element method to examine the fretting fatigue characteristics of untreated and plasma nitrided AISI 316L stainless steel. The results were found to be close to experimental results, indicating the method's suitability for determining fatigue results of plasma nitrided parts. In another study, Yildiz et al. [24] compared the fatigue life of TiAlN coatings experimentally and theoretically with the finite element method. They observed that the values obtained experimentally and from the finite element analysis were close. Sawicki et al. [25] used the FEA to simulate material behaviour during cyclic loading, introducing residual stress state from nitriding. The goal was to understand fatigue behaviour of nitride steel and improve numerical fatigue life predictions for residual stresses. The simulation results were compared with plane bending fatigue tests, suggesting the method could enhance fatigue analysis accuracy and service life optimization. In another work by Khairul et al. [26] a finite element model was developed to simulate and predict the lifespan of 316L stainless steel under ambient temperature. The model validated and compared fatigue lives with experimental results, showing slight differences. The model predicted maximum stresses slightly less than experimental ones and a drop in predicted fatigue strength due to material imperfections.

In the literature, numerous studies using finite element analysis have been performed to examine the impact of notches on fatigue performance of the materials, and depending on the size and form of the notch as well as the kind of material under study, different effects of notches have been seen. According to the pertinent research, studies on associating the fatigue performance of only plasma nitrided and only notched samples via the FEA are being rarely studied by researchers. Furthermore, to date, no comparative studies have been conducted on the mitigation of the notch effect through plasma nitriding. Therefore, the aim of this study is to examine the synergetic effects of PN and notches on the fatigue strength of AISI 4140 steel under constant amplitude loading, through experimental and numerical analyses. In keeping with this target, fatigue test samples made out of AISI 4140 steel, which were prepared in different radius sizes (R1, R2, R4, and R8 mm) was plasma nitrided at various temperatures. The mechanical and structural properties of plasma nitrided specimens were examined using SEM, XRD, fatigue and micro hardness tester. Fatigue tests were carried out using a rotational bending tests system and moreover, the notch fatigue resistance results of specimens were compared with the FEA results.

2. Experimental and numerical methods

2.1. Sample preparation, fatigue tests and characterizations

AISI 4140 low-alloy steel was used in the present study. The chemical compositions of the AISI 4140 samples were analysed using the Thermo Scientific Niton XL2 Plus brand XRF analyser and the chemical content is as follows: C: 0.41, Mn: 0.56, Si: 0.30, Cr: 0.90, P: 0.0.14 (wt.%). Table 1 shows the mechanical properties of AISI 4140 alloy. The notch fatigue test samples were produced on the CNC (Medical Consept Sağlik Turizm San. ve Tic. Ltd. Şti. Turkey) and their surfaces were polished. The notch geometry dimensions specimens with four different notch radii (1, 2, 4 and 8 mm) were designed, whose stress concentration factors (K_t) were 1.63, 1.41, 1.27 and 1.19, respectively [27,28]. The details of the produced samples, which were specially designed according to the ASTM E466-96 standard with the possibility of the rotating bending fatigue-testing machine, are shown in Fig. 1.

Table 1
The mechanical properties of AISI 4140 low alloy steel.

Young's Modulus, E (GPa)	Yield Stress, σ_y (MPa)	Ultimate Stress, σ_u (MPa)
205	420	650

Plasma nitriding processes were performed in an I-Nit industrial plasma nitriding system (İstanbul Isıl İşlem Ltd. Şti. Turkey). The nitriding process takes place with an electrical discharge between the cathode discs and the steel anode. Power unit and vacuum pump are used to create the necessary vacuum in the nitriding system. Before starting the nitriding process, the environment was vacuumed with the help of a vacuum pump. The temperatures of the test samples were measured with the help of the heat sensor connected to the cathode disk. The samples were placed vertically evenly spaced in the nitriding chamber. Since the samples at the cathode are symmetrical, the temperature taken from any sample is the same for other samples. The voltage, gas flow and temperature are adjusted to remain constant during the treatment period. Dirt, rust and unwanted substances that may be specimens were cleaned until the processing temperature was reached in the vacuum environment. Afterwards, it was accepted that the nitriding period started when the determined gas mixture and process temperature were reached. The plasma nitriding process parameters are given in Table 2.

The formed phases on the nitrided layer are investigated by XRD (GNR-Explorer) using Cu-K α ($\lambda = 1.5406$ nm) radiation (scanning angle:$30^\circ < 2\theta < 90^\circ$, and scanning speed: with an increment of 2°/min). The measurements of residual stresses were made performed using the XRD-GNR-Explorer system and the sin2ψ method [29]. Three different incident angles (ω) were used for the measurements: 5°, 10°, and 15°. Because it maximizes the detection of maximal residual stresses,—which are usually produced in sub-surface regions by procedures like plasma nitriding—these particular angles were selected. The cross section and fracture surfaces of the samples were examined by using ZEISS Sigma 300 and FEI Quanta FEG 250 scanning electron microscopes (SEM). The Vickers micro-hardness measurements were conducted by using Shimadzu HMV-G tester with a load of 50 g for 10 s. The fatigue tests of the specimens were carried out by using a RAAGEN brand rotating-bending fatigue system under room temperature (laboratory ambient condition) at a frequency of 50 Hz (3000 rpm) and a load ratio of $R = -1$. Heat generation at 3000 rpm in AISI 4140 steel specimens, particularly at the notches, is expected to be minimal due to the material's good thermal conductivity and high melting point. While some localized heat may occur at stress concentration points, the context does not indicate that this would significantly affect fatigue life. Plasma nitriding improves fatigue resistance by increasing surface hardness and introducing compressive residual stresses, which mitigate the negative effects of notches. Therefore, even if there is a slight temperature rise, it would have little to no effect on the service life of the specimens. In this system, the sample is rotated by compressing it from one end while it is subjected to force from the other end. Bending occurs when the specimen is subjected to a load from one end. The stresses resulting from bending of the fatigue specimen have been calculated through Eq. (1).

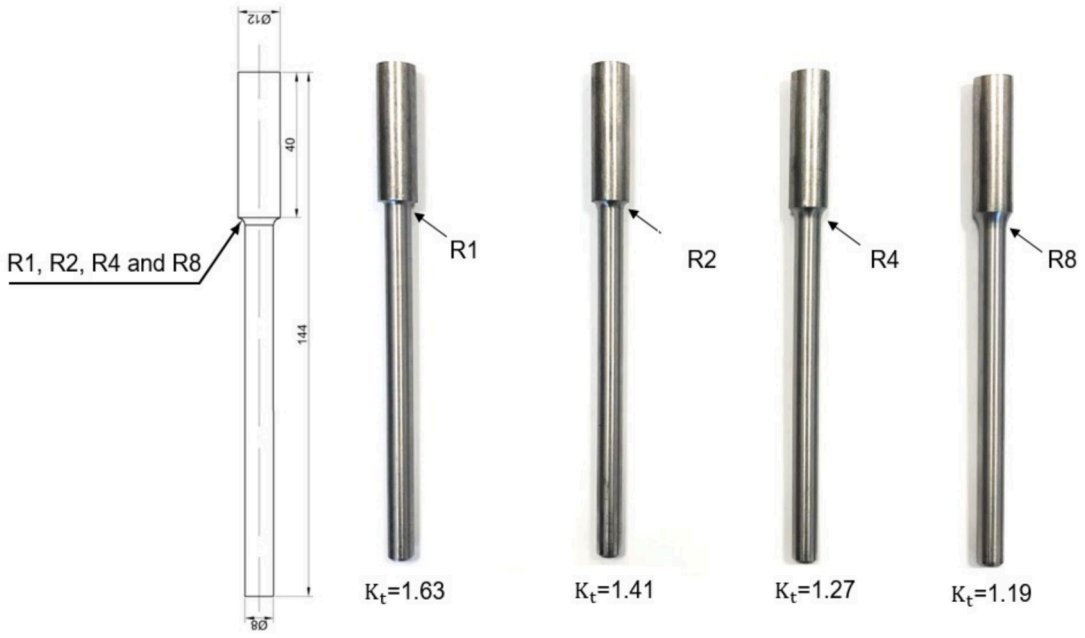

Fig. 1. Overview of the manufactured notch fatigue specimens.

Table 2
Plasma nitriding parameters of the fatigue test samples.

Samples	Gas mixture	Temperature, (°C)	Time, h
F1	20 % N_2 + 80 % H_2	460	9
F2	35 % N_2 + 65 % H_2	535	9

$$\sigma_g = \frac{M_e}{W_e} = \frac{F \times a}{\frac{\pi \times d^3}{32}} \quad (1)$$

Here, σ_g is the normal stress resulting from bending, M_e is the bending moment, W_e is the bending resistance moment of the section. In this study, it is seen that there is a relationship given in Eq. (2) between the applied load (F) and the stress formed in the critical section (σ_g). For example, when the test sample is 8 mm in diameter and 106 mm in moment arm length is placed in Eq. (1).

$$\sigma_g = 2F \quad (2)$$

In this investigation, fatigue tests were systematically conducted on AISI 4140 steel specimens, terminating either upon specimen failure or after reaching approximately 10^6 cycles, consistent with staircase methodologies. This staircase method was used to obtain S-N curves of the specimens. According to this method, two samples for each of the five stress amplitude levels and twelve samples for the infinite life region made up the total of 22 samples that were utilized to calculate the S-N curve for each group. The stress value that corresponded to the cycle at which the samples achieved at least 6×10^6 cycles was recorded as the endurance limit (fatigue strength), and this stress value was regarded as infinite life. Hence, fatigue strengths of the specimens were determined, as described elsewhere [5,30–32] The ASTM E739-91 standard was applied to facilitate the statistical analysis of the results, enabling the determination of the fatigue limit with a 95 % confidence interval [9,33].

2.2. Finite element analyses

Fatigue behaviour of untreated and plasma nitrided notched parts under constant amplitude loads were analysed using ANSYS Workbench

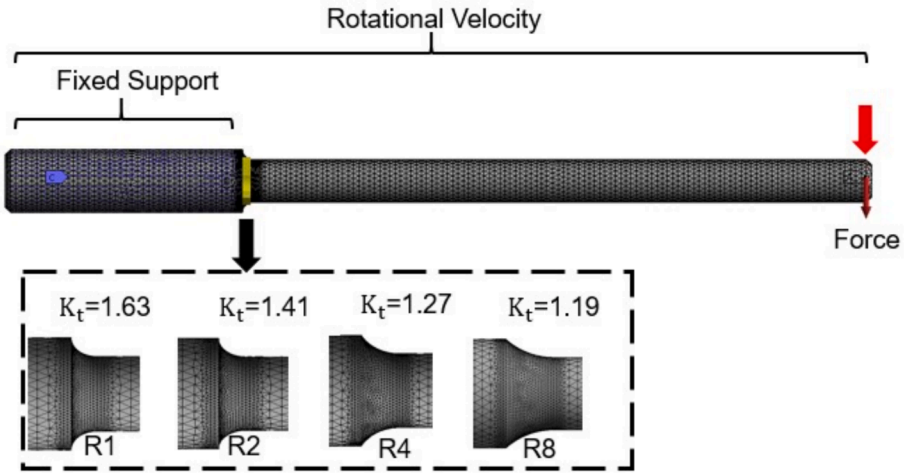

Fig. 2. Mesh generation and boundary conditions for FEA analyses.

Table 3
The mesh properties of notched samples.

Samples	Elements	Nodes	Mesh Method	Smoothening	Element quality
R1	101739	145238	Automatic	Medium	0.84
R2	116550	169524	Automatic	Medium	0.84
R4	121835	176945	Automatic	Medium	0.84
R8	133116	192871	Automatic	Medium	0.84

2020 R2 software, adapting a stress life approach. Stress life approach which is based on S-N curves is used [34,35]. The load and boundary conditions applied to certain points during the analytical calculation are given in Fig. 2. The simulation procedure involved executing various processes, including performing geometry operations, generating a finite element mesh, creating material models, applying load and boundary conditions, and reporting solutions and results. The elements used are tetrahedral 3D components. Here the mesh elements, nodes, method, smoothening, and element quality are given below in Table 3. Boundary conditions were applied to the notched samples after the mesh step. The fatigue specimen was firmly supported at one end, and a rotational speed of 3000 rpm was applied. Five different loads, which corresponds to each load level in each fatigue experiments of different samples, were used in the fatigue model, and the obtained life values were compared with the experimentally obtained life values. Similar steps have been followed for R1, R2, R4 and R8 notch models.

In order to determine the influences of plasma nitriding processes applied on materials on fatigue properties through finite element analysis, surface treated material properties should be transferred to the program. In FEA, it is not appropriate to consider the layers and the substrate independently of each other in terms of performing fatigue analysis. For that reason, the plasma nitrided material should be considered as a whole with substrate and layers. Therefore, Young's modulus of the plasma nitrided material must be imported into the program. In order to assess the fatigue life of surface treated materials via FEA a spring model was proposed by Guagliano and Vergani [36]. As shown in Fig. 3, material and surface layers were considered as parallelly connected springs and following this approach Young's modulus of surface treated materials can be calculated through Eq.3-Eq.5. The model in Fig. 3 is a simple model used for understanding the mechanical behaviour of a nitrided material. In this model, the outer layer of the material (nitrided layer) and the core are considered as two different springs. These springs have different elastic modules (E) and cross-sectional areas (A) and are connected in parallel. Terms used in the model are as follows: K: spring constant represents the stiffness of the material. E: elastic modulus represents the elasticity of the material. A: the cross-sectional area represents the geometric size of the material. In the model, total hardness (K_{Total}) is calculated according to Eq. (3). Here, $K_{Substrate}$ and K_{Layer} are the spring constants for the outer layer and core, respectively. Using the elastic moduli and cross-sectional areas, these values are calculated by Eq. (5).

In this regards, elastic modulus profiles of AISI 4140 steel subjected to plasma nitriding under various gaseous mixtures and temperatures are analysed using nanoindentation. Measurements were conducted at 15 different points on each sample surface, employing a range of loads from 25 down to 1.6 mN, resulting in a comprehensive set of penetration depth readings for each load level. To address the challenges posed by surface roughness, initial tip contact points were rectified by analysing contact stiffness curves, thus accurately determining the zero depth position. This adjustment ensured that the subsequent recalculations of elastic modulus profiles, via the refined Oliver–Pharr method accurately reflected the nuanced properties of the nitride-altered surfaces [37–39]. Additionally, an enhanced version of the Pharr technique was utilized to minimize statistical errors, further ensuring the precision of the mechanical property evaluations [35]. After plasma nitriding, a material typically develops both a compound layer and a diffusion zone. For the purpose of simplicity in analysis, these two regions can be considered as a single layer when calculating the elastic modulus. Nanoindentation testing, therefore, becomes an ideal method for evaluating the surface mechanical properties of such treated materials, offering minimal

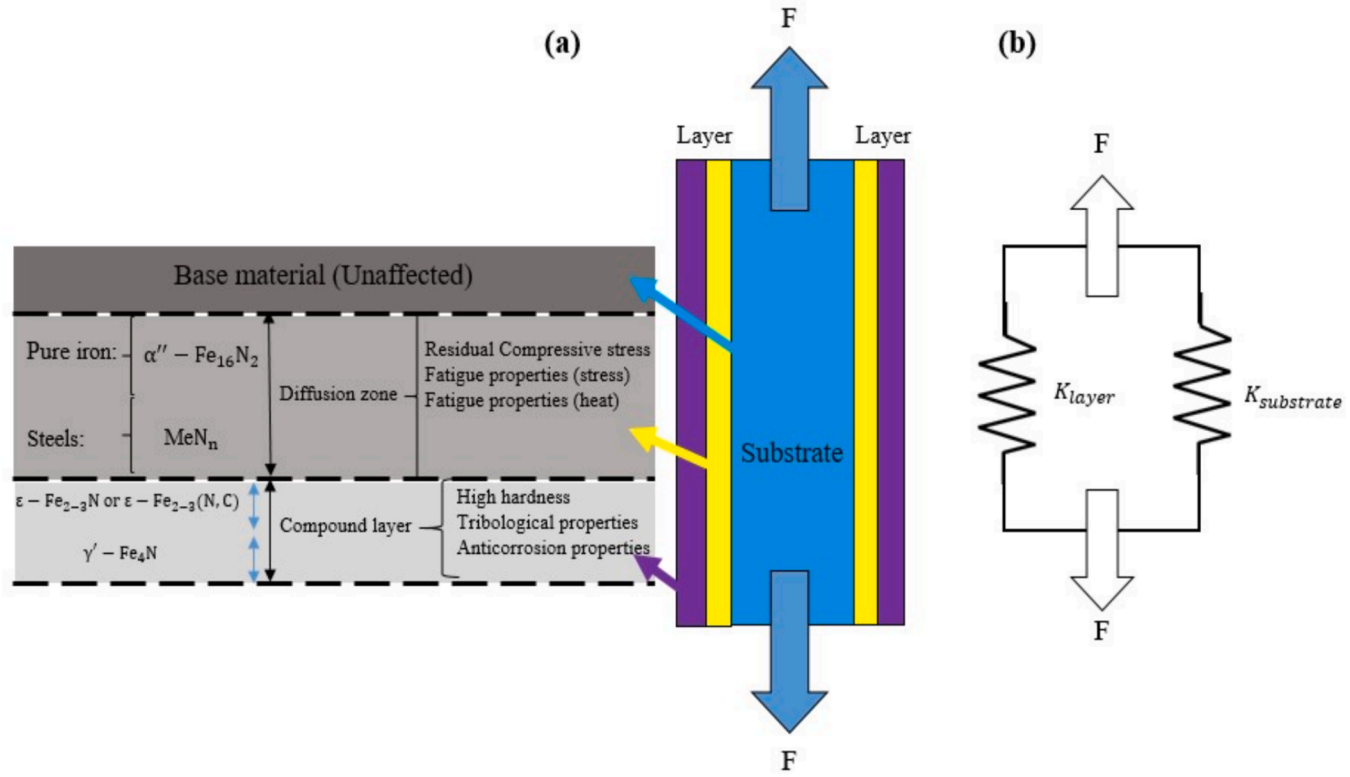

Fig. 3. The spring model for surface treated materials: a) Schematic illustration of nitrided materials and b) spring model [24].

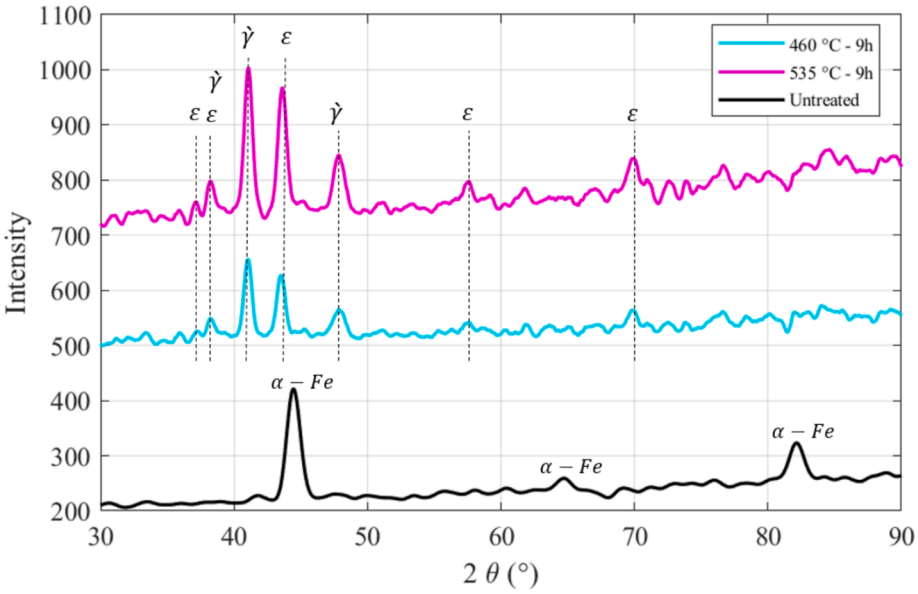

Fig. 4. XRD spectra of untreated and plasma nitrided samples.

interference from the bulk structure. Through this approach, the elastic modulus (E) is determined by analysing the relationship between the load applied and the penetration depth of the indenter, allowing for precise characterization tailored to the nuanced surface behaviour created by plasma nitriding. Accordingly, the elastic modulus values of the tested samples were evaluated using the nanoindentation technique, which allows precise measurement.

Considering the nanoindentation measurements of the notched components in this current research, for fatigue specimen properties, physical and mechanical properties (ρ = 7850 kg/m^3, melting point = 1416 °C, thermal conductivity = 46.2 W/m-k) of untreated AISI 4140 steel (E = 210 GPa, ϑ=0.3, σ_{yield}=415 MPa) were used, respectively [36,40]. The elastic modulus of nitrided materials is calculated using a spring model (Eq. (3), which treats the nitrided layer and the core material as two parallel springs with different stiffness values. This model accounts for the combined mechanical behaviour of the nitrided layer and the substrate. Nanoindentation techniques are used to measure the elastic modulus of the nitrided layer. This method provides precise measurements of surface mechanical properties by analysing the relationship between the applied load and the penetration depth of an indenter. The elastic modulus values for nitrided samples depend on the thickness of the nitrided layer. For example, the F1 sample has a 250 μm nitrided layer, while the F2 sample has a 320 μm nitrided layer. Using the spring model (Eq. (3), the elastic modulus of the F1 sample is calculated as 230 GPa, and the F2 sample as 260 GPa. These values reflect the increased stiffness of the material due to the thicker nitrided layer in the F2 sample. The detailed information about the finite element analysis can be found in [23]. These elastic modulus values are crucial for estimating the fatigue life of the samples. The fatigue life is determined by analysing the stress distribution and deformation behaviour under cyclic loading, which depends on the material's stiffness. The elastic modulus of nitrided materials, such as the F1 and F2 samples, is calculated using a spring model (Eq. (3), which considers the nitrided layer and the core material as two parallel springs with different stiffness values. This approach allows for an accurate representation of the combined mechanical behaviour of the nitrided layer and the substrate. Nanoindentation techniques are employed to measure the elastic modulus of the nitrided layer, providing precise data on surface mechanical properties. For the F1 sample with a 250 μm nitrided layer, the elastic modulus is calculated as 230 GPa, while for the F2 sample with a 320 μm nitrided layer, it is 260 GPa. These values indicate that the thicker nitrided layer in the F2 sample results in greater stiffness. The elastic modulus values are essential for estimating the fatigue life of the samples, as they influence the stress distribution and deformation behaviour under cyclic loading. The finite element analysis (FEA) model incorporates these values to simulate the material's response to cyclic loading and predict fatigue life. The results from FEA are compared with experimental data to validate the model and ensure accurate predictions. This analysis highlights the importance of understanding the mechanical properties of nitrided materials for improving their fatigue performance.

This model is used to understand stress and deformation behaviours in different regions of the material. In particular, the different elastic moduli of the outer layer and the core cause the stress profile to be non-uniform. This can cause the outer layer to stretch more than the core. The model is used to understand how these differences affect the material's fatigue behaviour. In particular, in low-cycle fatigue tests, this model is used to describe the fracture behaviour of the outer layer and crack initiation points.

$$K_{Total} = K_{Substrate} + K_{Layer} \tag{3}$$

$$\frac{E_{Total}A_{Total}}{L} = \frac{E_{Substrate}A_{Substrate}}{L} + \frac{E_{Layer}A_{Layer}}{L} \tag{4}$$

$$E_{Total} = \frac{E_{Substrate}A_{Substrate} + E_{Layer}A_{Layer}}{A_{Total}} \tag{5}$$

3. Results and discussions

3.1. Structural characterization

XRD spectra of untreated and plasma nitrided samples are shown in Fig. 4. It is seen that untreated specimen shows only α-Fe peaks, whereas γ′-Fe_4N (face-centred cubic) and/or ε-$Fe_{2\text{-}3}N$ (hexagonal close packed) phases are formed in the samples after plasma nitriding [41,42]. ε-$Fe_{2\text{-}3}N$ and γ′-Fe_4N phases increase as the plasma nitriding temperature does (Fig. 4). In the literature, it has been reported that the intensity of γ′-Fe_4N increases, but the ε-$Fe_{2\text{-}3}N$ phases decrease with the increase of the PN temperature. PN time is much more effective than temperature in the formation of the intensity of the ε-$Fe_{2\text{-}3}N$ and γ′-Fe_4N phases. As the processing time increases, more nitrogen atoms diffuse into the material. This enhanced diffusion leads to the formation of iron nitride phases.

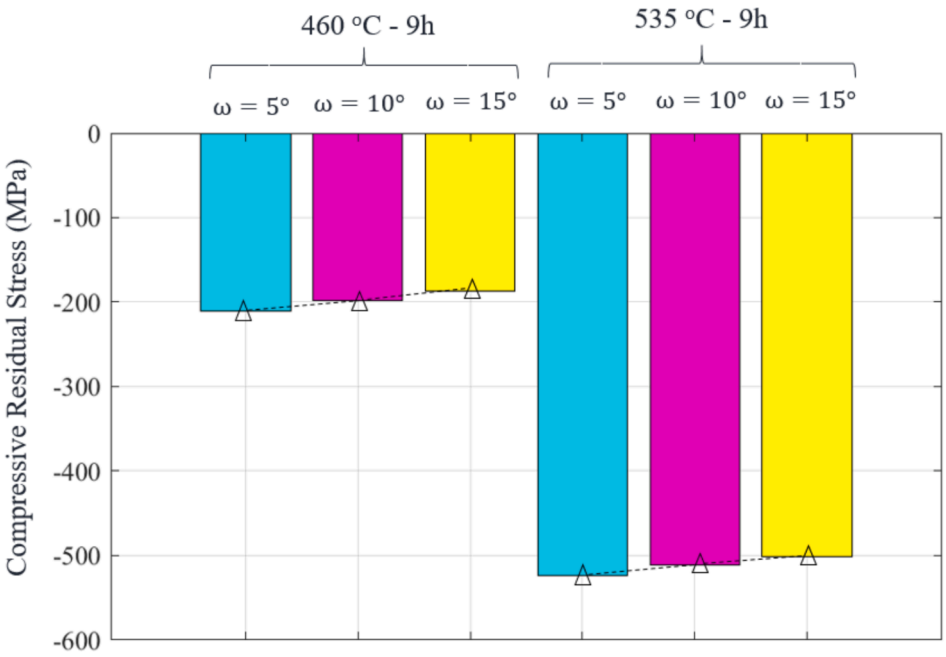

Fig. 5. Residual stresses measured from plasma nitrided specimens.

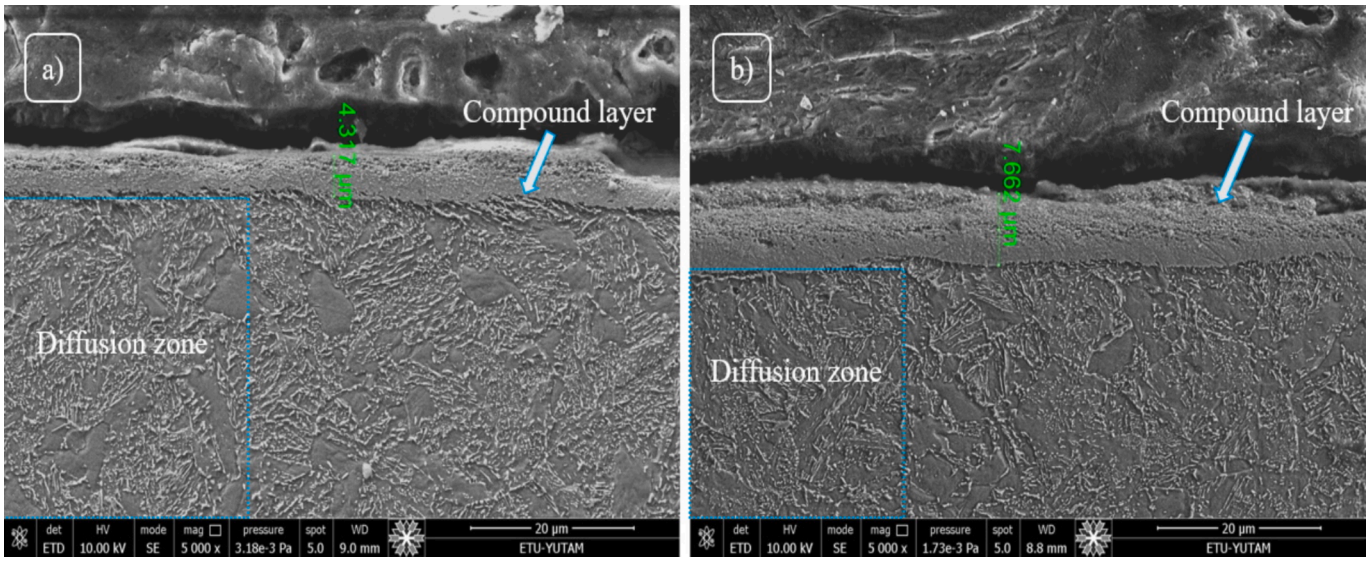

Fig. 6. SEM images showing the cross section of the samples: **a)** F1 and **b)** F2.

Consequently, the peak intensities of these iron nitride phases increase with longer treatment durations. This relationship indicates that prolonged processing time promotes the formation and growth of iron nitride phases within the material [43,44].

The residual stress values of plasma nitrided samples at different incidence angles are shown in Fig. 5. Initially, the surface residual stress of the F1 sample is −211 MPa. However, with increasing nitriding temperature, the maximum residual stress was observed in the F2. It has been noted that the application of a higher process temperature leads to an increase in compressive residual stresses. Furthermore, the nitrogen atoms exhibit greater diffusion when the temperature increases (Fig. 5). Therefore, it is believed that there are aberrations in the lattice structure of the atom, leading to increased residual stresses [45,46]. Residual stresses in a modified layer after plasma nitriding tend to decrease from the surface towards the core due to the characteristics of the diffusion mechanism. To assess the variations in residual stress, three distinct glancing angles were employed. When measurements are taken at higher glancing angles, the X-Ray beams penetrate deeper into the material. Consequently, measurements taken at these higher angles yield lower residual stress values.

The PN method involves a bilayer structure on the sample surface, comprising two distinct sections that contain the nitride phases (Fig. 6). The compound layer, a hard, thin, and brittle component, is generated alongside the diffusion layer, which extends from the material surface to the core of the materials [47]. It was observed that the thickness of the structure developed on the specimens grew from 4.3 µm to 7.6 µm, as the temperature increased. This phenomenon is attributed to the process of nitrogen diffusing into the steel and subsequently forming finely scattered nitrides.

Based on the microhardness outcomes, the untreated sample exhibited an average hardness value of 210 $HV_{0.5}$. The surface hardness is approximately 471 $HV_{0.5}$ in F1, while it is 550 $HV_{0.5}$ in F2 (see Fig. 7).

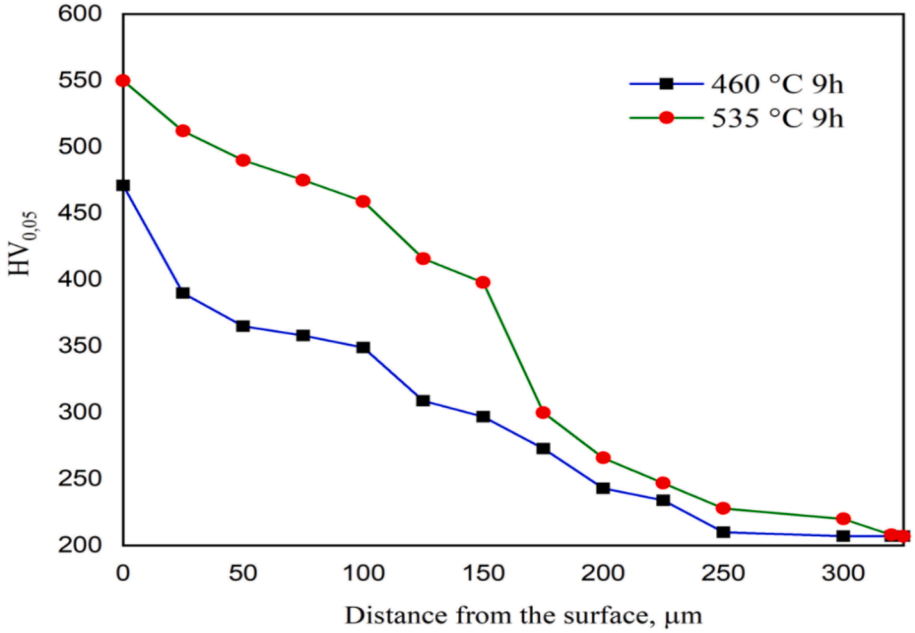

Fig. 7. Micro hardness profiles of plasma nitrided samples.

Table 4
The S-N equations, 95% confidence interval of fatigue limit and the fatigue limit values for all fatigue test conditions for 10^6 cycles.

Specimens	Equation of S-N curve	95 % Confidence interval	Fatigue limit at 10^6 cycles (MPa)	*Change in fatigue limit %
Untreated-r1	$LogN = 37,34024-(12,41741 \times logS)$	320–341	334	–
Untreated-r2	$LogN = 34,01508-(10,99910 \times logS)$	335–360	352	–
Untreated-r4	$LogN = 47,73601-(16,09242 \times logS)$	385–405	392	–
Untreated-r8	$LogN = 76,83673-(27,03721 \times logS)$	388–433	417	–
F1-r1	$LogN = 59,11817-(19,81248 \times logS)$	450–495	480	+47
F1-r2	$LogN = 87,76740-(29,47609 \times logS)$	525–570	550	+50
F1-r4	$LogN = 89,12417-(29,32334 \times logS)$	542–605	584	+53
F1-r8	$LogN = 92,97404-(30,89379 \times logS)$	620–676	654	+60
F2-r1	$LogN = 109,50593-(36,83054 \times logS)$	659–672	646	+88
F2-r2	$LogN = 117,78810-(39,32408 \times logS)$	695–725	696	+89
F2-r4	$LogN = 163,14752-(53,98007 \times logS)$	802–856	815	+110
F2-r8	$LogN = 163,63980-(56,76225 \times logS)$	828–897	855	+110

* "The values of % change in fatigue limit'' is calculated with reference to the fatigue life of each notch geometry in the untreated state.

An increase in surface hardness is seen due to the formation of a compound layer containing a significant amount of the ε-$Fe_{2-3}N$ phase and the resulting rise in layer thickness. The surface hardness is directly proportional to the ratio of Ɛ to γ′ [48]. Microhardness measurements were conducted at various depths from the surface to the core of the sample to determine the substrate hardness, which also indicated the diffusion depth. The highest hardness values were recorded in the regions closest to the surface. It was observed that increased nitriding times and temperatures resulted in greater diffusion depths, leading to higher hardness values and thicker modified layers. Furthermore, it was determined that the treatment temperature had a more significant impact on enhancing both surface and subsurface hardness compared to the treatment duration. It is understood from the figure that the diffusion zone has a depth of 250 µm and 320 µm for F1 and F2 specimens, respectively. The depth of the diffusion zone is greater under F2 conditions compared to other condition.

3.2. Fatigue and fracture examinations

The fatigue limits of the samples are given in Table 4 and the percentage changes in fatigue limits of untreated and plasma nitrided samples are shown in Fig. 8. Fig. 8 shows the effect of plasma nitriding on the fatigue strength of notched parts by showing the increasing ratio (%) for different notch radii. Plasma nitriding significantly increases the fatigue strength of notched parts at all notch radii. The plasma nitrided samples (F1 and F2) show consistently higher increasing ratios compared to the untreated ones. As the notch radius increases, the effectiveness of plasma nitriding in improving the fatigue strength also increases. For example, the increase is more pronounced at larger radii (R4 and R8) than at smaller ones (R1 and R2). The F2 process generally results in a higher increase in fatigue strength compared with F1, indicating that certain parameters of the F2 process are more effective. In general, plasma nitriding is beneficial to improve the fatigue strength of notched parts, and its effectiveness increases with larger notch radii.

The fatigue performance of the plasma nitrided-notched specimens exhibited superior characteristics compared to the untreated notched specimens. The fatigue resistance of R1 ($K_t = 1.63$) notched AISI 4140 steel was increased approximately 47 % and 88 % after the nitriding treatment (as also shown in Fig. 9-a. Fig. 9-b shows that the fatigue strength of R2 ($K_t = 1.41$) notched AISI 4140 steel increases by 50 % and

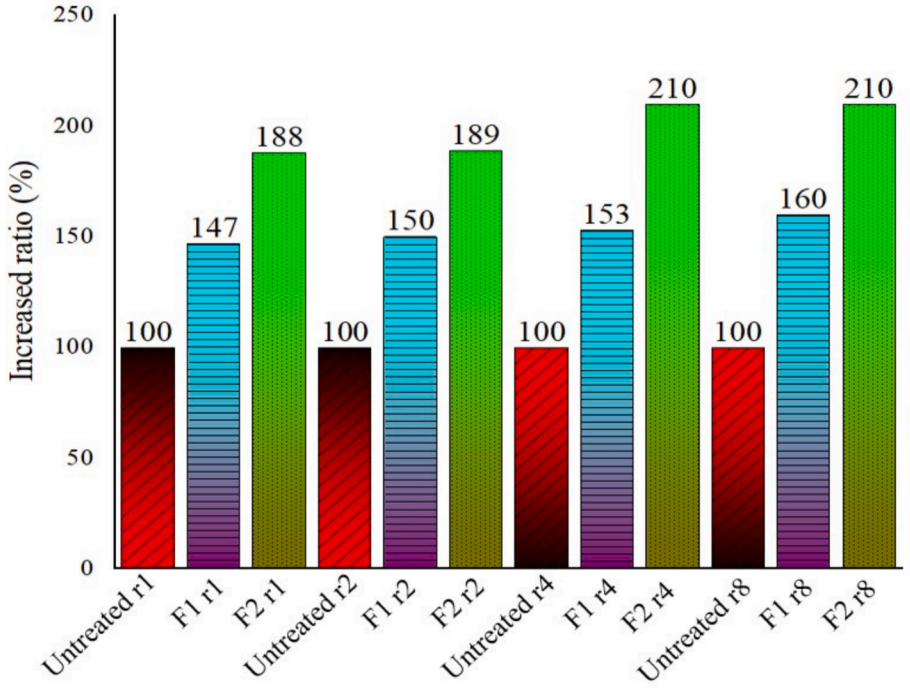

Fig. 8. The changes in fatigue limit of untreated and plasma nitrided samples.

89 % after the nitriding process. The nitriding treatment resulted in an approximate increase of 53 % and 110 % in the fatigue resistance of AISI 4140 steel with a notch factor of $K_t = 1.27$, as demonstrated in Fig. 9-c. Fig. 9-d illustrates that the fatigue strength of R8 (with a stress concentration factor of 1.19) notched AISI 4140 steel experiences a 60 % and 110 % increase following the nitriding process. The untreated material has a shorter fatigue life compared to the strengthened materials with plasma nitriding. It shows how plasma nitriding modifies the material surface and increases fatigue strength. The material treated in the F1 condition exhibits significantly higher fatigue strength than the untreated condition. This is possible by optimum adjustment of the process temperature, time and process parameters. It demonstrates how plasma nitriding at higher temperatures affects fatigue performance. The F2 condition generally offers a higher fatigue resistance compared to F1, but in some cases undesirable microstructural changes may also occur due to excessive temperature effects.

The S-N curves of untreated and plasma nitride samples are shown in Fig. 9. These curves compare the fatigue behaviour of different notch types (R1, R2, R4, R8) after plasma nitriding. Each graph contains experimental and numerical results. In all notch types, the untreated condition has the lowest fatigue resistance. Experimental and numerical results are generally compatible, and fewer cycle fractures are observed at low stress levels. At F1 condition, fatigue resistance increases for all notch types. However, this increase is more pronounced for R1 and R2 notches. Experimental and numerical data are often close to each other. Condition F2 provides the highest fatigue resistance of all notch types. This effect is more evident in the R4 and R8 notches, and a good agreement is observed between the experimental and numerical results. As a result, the plasma nitriding process increases fatigue resistance in all notch types. At the notch root, where stress amplitude is relatively high, cyclic work hardening typically occurs due to localized plastic deformation. However, plasma nitriding mitigates this effect by strengthening the material surface and reducing stress concentration. The study highlights that the fatigue resistance improvement is more pronounced in larger notches (R4 and R8) under the F2 condition, where the material undergoes higher surface hardening and compressive stress. This suggests that plasma nitriding minimizes the impact of cyclic work hardening by enhancing the material's ability to withstand cyclic loading without significant degradation in strength properties. While the F2 condition provides the highest resistance levels, experimental and numerical results generally proceed in agreement. These findings highlight the importance of plasma nitriding in materials design and applications.

SEM fractography of plasma nitride samples are shown in Fig. 10. These images are scanning electron microscope (SEM) images that examine a material's microscopic structure and fracture behaviour. Each image shows different features and defects. Such analyses are important for understanding the mechanical properties and durability of the material. Fig. 10-a reveals the fracture image of the R2 ($K_t = 1.41$) notched sample with the F2 plasma nitriding process. Here, the specimen was subjected to a cyclic stress of 720 MPa until it fractured completely after 480,361 cycles. It is understood from here that the image reveals the surface morphology of the material after fracture in detail. The smoothness and homogeneous structure on the fracture surface show the effect of the hardened layer formed by the plasma nitriding process on the material. The PN process has significant influences on the fatigue limit of the samples. However, fatigue cracking originated from the surface in some samples. This causes the multi-phase compound layer to be brittle due to its high hardness [49]. The fracture surface of the R4 ($K_t = 1.27$) notched sample with the F1 plasma nitriding process, loaded under 600 MPa cyclic stresses up to complete fracture at the failure cycle of 780,029 is shown in Fig. 10-b. The fracture image of the R4 (Kt = 1.27) notched sample with the F1 plasma nitriding process, broken under the influence of is shown in Fig. 10-c, resulted from 169,036 cycles under a load of 560 MPa. It shows the points where cracks begin and microcracks on the surface of the material. Crack initiation points represent weak areas of the material, and stress concentration in these areas affects the fracture behaviour. The plasma nitriding process increases the mechanical strength of the material by minimizing the formation of such microstructural defects. Fig. 10-d shows the SEM image of the internal structure of the F2 plasma nitriding process applied to the R8 ($K_t = 1.19$) notched part after the fatigue tests. The specimen endured a cyclic stress of 880 MPa, ultimately fracturing completely after 555,555 cycles, showcasing the material's fatigue resistance under high-stress conditions. It can be seen that the micro-voids formed within the material. These voids represent weak points in the internal structure

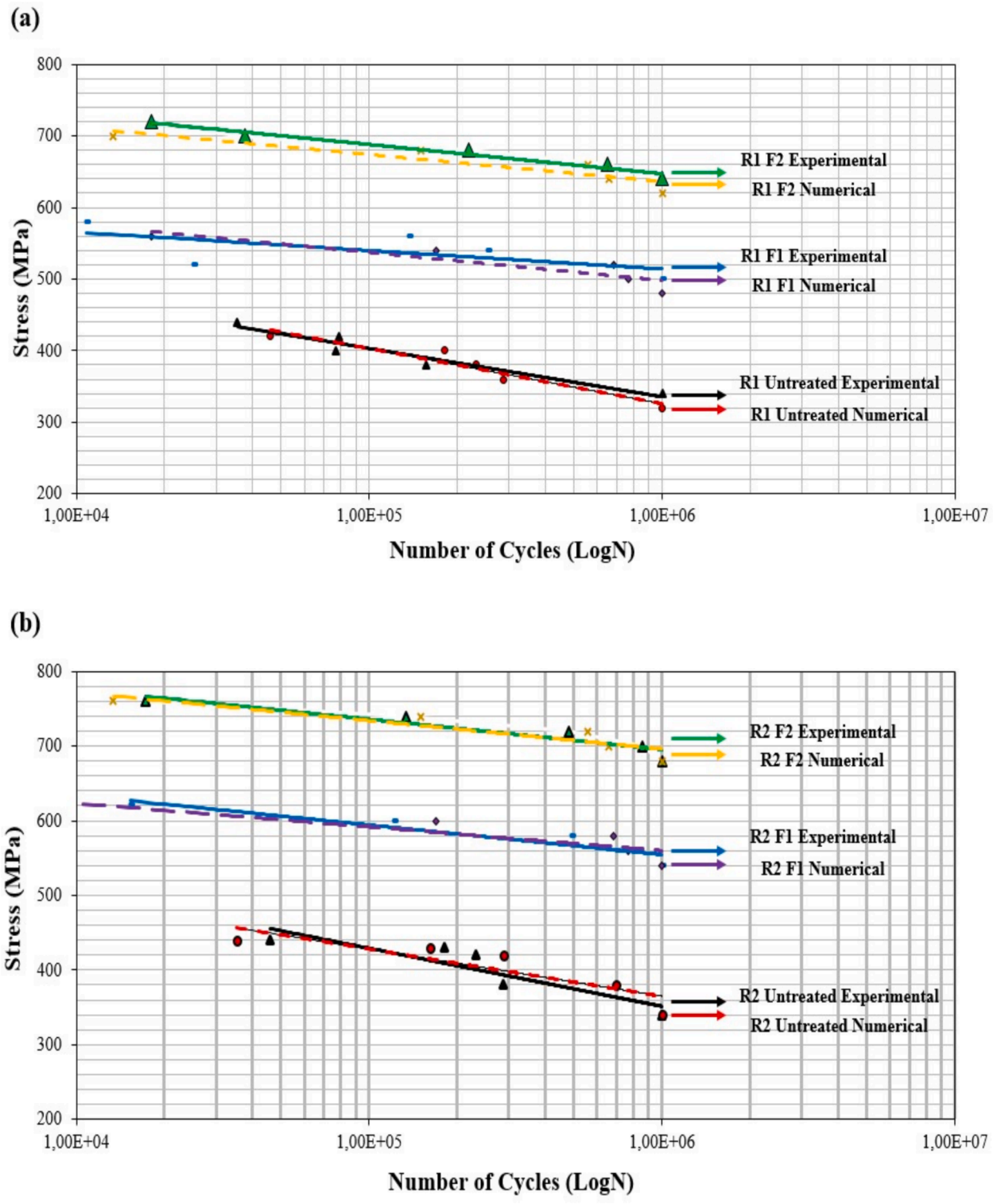

Fig. 9. Experimental and numerical S-N curves of untreated and plasma nitrided specimens: **a)** R1, **b)** R2, **c)** R4 and **d)** R8 notched.

of the material and can negatively affect fracture behaviour. The nitriding process increases the overall durability of the material by reducing the formation of such microstructural defects. As expected, the fatigue resistance increased in plasma nitrided samples. These evidences confirms that the increased hardness and residual stress caused by nitriding greatly delay the occurrence of surface fracture development. In general, the core portion of the samples is primarily characterized by a prevalent transgranular ductile fracture [50,51].

3.3. Finite element analysis results

Static analysis is performed before fatigue analysis to prove that the stress due to the load is well below the yield point of the specimens. Fig. 11 shows the simulation images of the strain, von Mises stress,

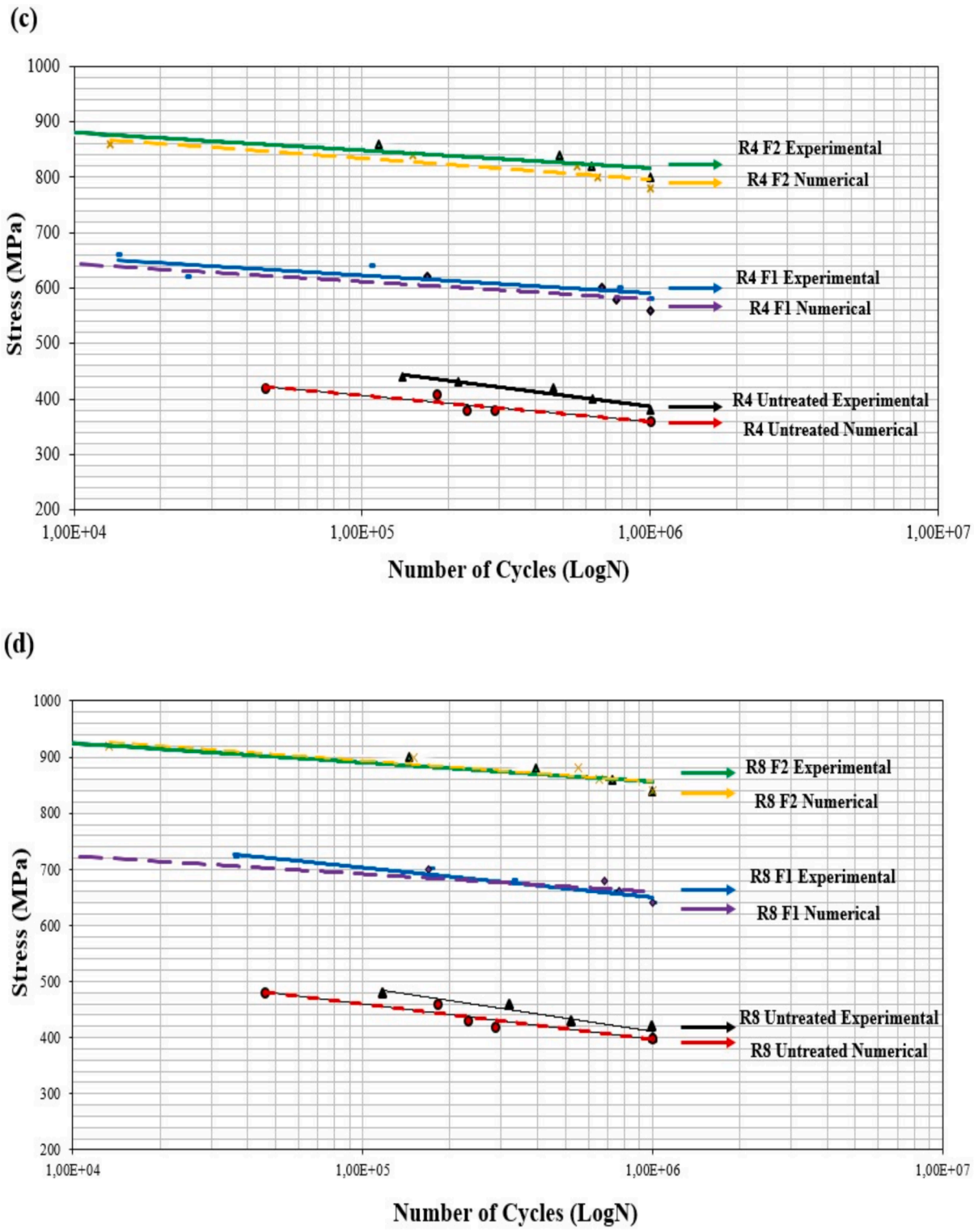

Fig. 9. (*continued*).

equivalent strain distributions and fatigue resistance of the fatigue specimen under 480 MPa static loading. It has the lowest values of total deformation (0.28 mm) and von-Mises stress (73.89 MPa). This notch shows less stress concentration than the others. Total deformation was calculated as 0.49 mm and von Mises stress was calculated as 132.21 MPa. R2 shows higher stress and deformation compared to R1. With 0.57 mm total deformation and 138 MPa von-Mises stress, R4 exhibits similar performance to R2. It has the highest total deformation (1.12 mm) and von Mises stress (254 MPa) values. These values are expressed in loading cycles and are determined through fatigue analysis, typically based on stress-life (S-N) criteria or other fatigue failure criteria. The fatigue life contours show how many cycles a specific region of the sample is expected to endure before failure initiates. Regions under higher stress (as indicated in the "Equivalent (von-Mises) Stress" plots) will generally have a shorter fatigue life. Colours in the contour map represent ranges of life (in cycles). For instance: Red indicates the

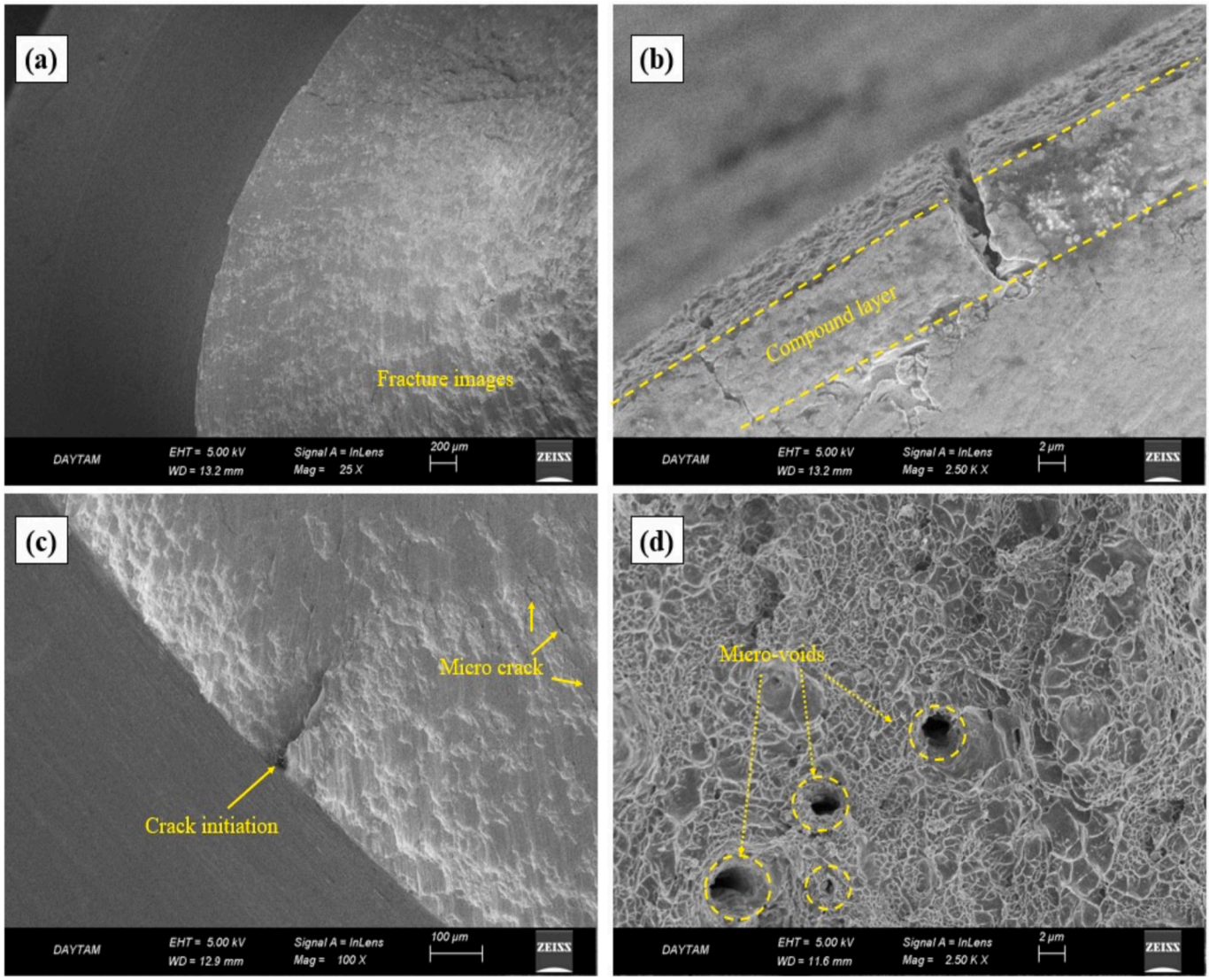

Fig. 10. SEM fractography of plasma nitrided samples.

shortest life (earliest failure). Blue represents regions with the longest anticipated fatigue life (often outside the influence of stress concentration). For all cases (R1, R2, R4, and R8), the minimum life (shortest cycles) occurs at the notched regions due to stress concentration. Conversely, areas farther from the notched zones exhibit higher life values because they experience significantly lower stress. On the other hand, this notch shows the highest stress concentration and deformation. The study reveals that notch geometry has a significant impact on mechanical performance. R8 notch shows the highest performance with the lowest stress and deformation values. These findings highlight the need for careful consideration of notch geometry in engineering designs.

Notched components are prone to fatigue failures due to the size effect and uneven stress distribution caused by the notches, leading to significant differences between Finite Element Analysis (FEA) and experimental results [52,53]. These discrepancies can be attributed to several factors. The FEA often employs idealized material properties and makes simplifications, such as linear elastic assumptions, which do not account for the real-world variability found in materials, such as microstructural defects or surface roughness. Additionally, FEA models typically rely on meshing and mathematical approximations, which might not accurately replicate the complex stress distributions induced by notches, particularly affecting larger components where material heterogeneities can alter stress concentrations. Moreover, challenges in precisely matching boundary conditions and loading paths between simulations and physical tests can lead to variations in observed fatigue life. Consequently, these factors emphasize the importance of correlating and validating FEA models with experimental data to enhance reliability and accuracy in predicting the fatigue behavior of notched components. After undergoing the plasma nitriding process, iron nitride phases gather on the surface and transform into interstitial atoms within the lattice structure of the material. This leads to the distortion of the lattice structure, leading to an augmentation in surface hardness and the presence of compressive residual stresses. The increased hardness and compressive residual stresses impede the movement of dislocations on the material surface. The prevention of dislocation movement leads to an increase in the fatigue life of the materials [54,55]. In our previous work [33], we found that the notch fatigue resistance may be enhanced by up to 72 % by the augmentation of layer thickness, surface hardness, and compressive residual stress distribution achieved by prolonging the nitriding process. For the mentioned reasons, an increase in notch fatigue resistance is expected after the PN process. Consequently, the endurance limit of both untreated and plasma nitrided notched samples reduced as the K_t (stress concentration factor) increased. Regarding this matter, the lifetime values of untreated and plasma nitrided-notched samples were experimentally compared with the predicted endurance limit derived using Finite Element Analysis (FEA) (Fig. 8). According to

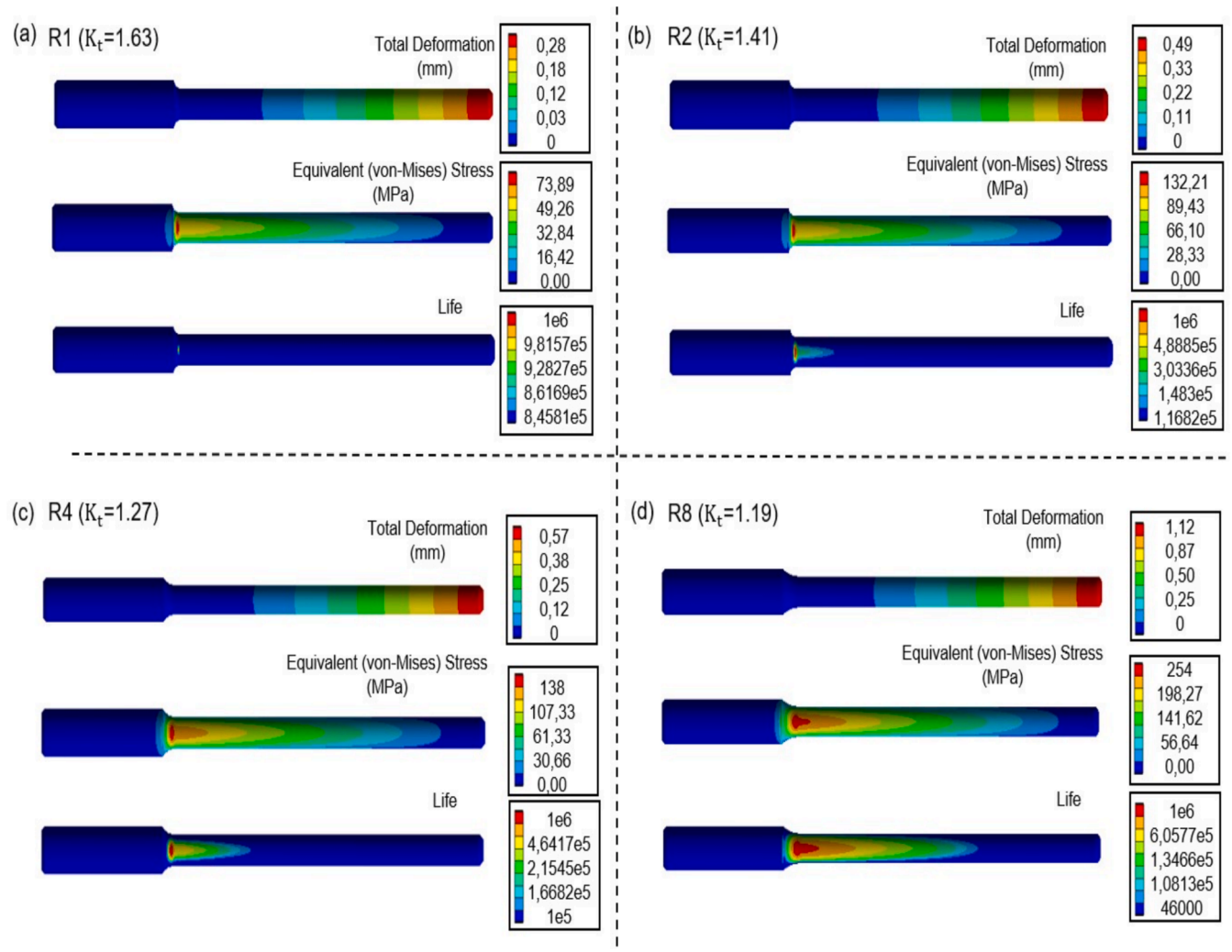

Fig. 11. FEA results of the fatigue test samples: **a)** R1, **b)** R2, **c)** R4 and **d)** R8.

the results obtained, it has been observed that there are acceptable errors between the experimentally obtained values and the values obtained from the finite element analysis. As a result, it was understood that the approach proposed Ref [36] and the model created gave positive results. The discrepancies between finite element analysis (FEA) and experimental results are often attributed to the inherent complexities and variabilities present in real-world materials and conditions, which are not fully captured by theoretical models. Material defects, such as voids and micro-cracks, along with surface variations introduced by treatments like plasma nitriding or TiAlN coating, significantly influence mechanical properties and fatigue behaviour [2023]. These factors are often simplified or omitted in FEA models. For instance, the studies on AISI 4140 steel reveal that while FEA provides a structured approach to predict fatigue life, it may not account for the nuanced effects of residual stresses and microstructural changes induced by surface treatments. Additionally, the assumptions regarding boundary conditions and loading scenarios in FEA can differ from experimental setups, leading to variations in stress distributions and fatigue predictions. The literature further suggests that the interaction between substrate and coating, particularly in terms of adhesion and hardness, plays a crucial role in fatigue performance, which is often challenging to model accurately [56–58]. Therefore, while FEA is a powerful tool for understanding material behaviour, its limitations necessitate careful interpretation alongside experimental data to ensure accurate and reliable engineering applications.

4. Conclusions

In the present study, the fatigue behaviour of notched AISI 4140 parts following plasma nitriding (PN) using different processing parameters were investigated comparatively through experimental tests and finite element analyses. The main findings of the study are summarized as follows:

- Following the surface treatment process, a compound layer composed of ε: ($Fe_{2\text{-}3}N$) and γ′: (Fe_4N) phases was generated on the surface of the material. Additionally, a diffusion layer with a high concentration of nitrogen atoms was developed beneath it. The intensity of the nitride peaks also augmented with the rise in nitriding temperature. The F1 and F2 samples had surface hardness values of 471 $HV_{0.5}$ and 550 $HV_{0.5}$, respectively, after nitriding. The XRD results showed that residual stress values increased with increasing nitriding temperature. Also, the highest values of residual stresses obtained at high incident angle ($\omega = 15^{\circ}$) were observed in the plasma nitrided F2 samples.
- The fatigue failure analyses of notched components were significantly impacted by the size effect, the uneven stress distribution caused by notches. It is detected that the F2 plasma nitrided specimens increased the average fatigue strength values by 88 % in R1, 89 % in R2, 110 % in R4, and 110 % in R8.
- Plasma nitriding enhanced the fatigue strength of material. The fatigue lifespan of plasma nitrided F1 and F2 samples increased in the

range of 47 and 110 %, respectively, compared to for the untreated ones. F2 plasma nitriding applications to R4 notched specimens are the most effective solution in engineering designs. The structural interaction between the notch geometry and the plasma nitriding process has a critical role on the fatigue strength of machine components.

- When the fatigue resistance values obtained after the FEA were compared with the fatigue resistance values obtained from the experimental results, it was determined that the fatigue curves were close to each other. The experimental and numerical findings are combined, and a consistent alignment between the results is noted.

CRediT authorship contribution statement

F. Yılan: Writing – original draft, Visualization, Validation, Methodology, Investigation. **H. Kovacı:** Writing – original draft, Supervision, Methodology, Investigation, Conceptualization.

Declaration of competing interest

The authors declare that they have no known competing financial interests or personal relationships that could have appeared to influence the work reported in this paper.

Acknowledgement

The authors would like to thank Prof. Dr. Ayhan Çelik, Prof. Dr. A. Fatih Yetim, Atatürk University East Anatolia High Technology Application and Research Center (DAYTAM) and Erzurum Technical University High Technology Application and Research Center (YUTAM) for their assistance.

Data availability

The authors are unable or have chosen not to specify which data has been used.

References

[1] S.R. Daniewicz, D.H. Moore, Increasing the bending fatigue resistance of spur gear teeth using a presetting process, Int. J. Fatigue. 20 (1998) 537–542, https://doi.org/10.1016/S0142-1123(98)00025-5.
[2] R.S. Rooprai, H. Singh, T. Singh, Y.K. Singla, Analysis of the wear properties of through hardened AISI-4140 alloy steel using Taguchi technique, Mater. Today Proc. 50 (2021) 661–664, https://doi.org/10.1016/j.matpr.2021.04.196.
[3] S. Pedroso, A. Mendes, A. José, R. Gonçalves, Enhancing the fatigue strength of AISI 4140 steel through in - situ urea - assisted EDM nitriding, Int. J. Adv. Manuf. Technol. (2024), https://doi.org/10.1007/s00170-024-14651-z.
[4] H. Çelik, H. Kovacı, Combined effects of magnetic field and surface treatments consisting of shot peening, plasma nitriding and their consecutive application on the friction and wear behavior of a ferromagnetic steel, Mater. Today Commun. 37 (2023) 107467, https://doi.org/10.1016/j.mtcomm.2023.107467.
[5] A.F. Yetim, H. Kovacı, H. Tekdir, Y.S. Kavasoğlu, Y.B. Bozkurt, A. Çelik, Enhancing high cycle fatigue performance of plasma nitrided AISI 4140 steel by post-aging treatment and direct current magnetic field, Mater. Today Commun. 40 (2024), https://doi.org/10.1016/j.mtcomm.2024.109704.
[6] K. Genel, M. Demirkol, M. Ürgen, Effect of cathodic polarisation on corrosion fatigue behaviour of ion nitrided AISI 4140 steel, Int. J. Fatigue. 24 (2002) 537–543, https://doi.org/10.1016/S0142-1123(01)00114-1.
[7] X.Q. Zhang, H. Li, X.L. Yu, Y. Zhou, S.W. Duan, S.Z. Li, Z.L. Huang, L.S. Zuo, Investigation on effect of laser shock processing on fatigue crack initiation and its growth in aluminum alloy plate, Mater. Des. 65 (2015) 425–431, https://doi.org/10.1016/j.matdes.2014.09.001.
[8] A. Weidner, T. Lippmann, H. Biermann, Crack initiation in the very high cycle fatigue regime of nitrided 42CrMo4 steel, J. Mater. Res. 32 (2017) 4305–4316, https://doi.org/10.1557/jmr.2017.308.
[9] S.Y. Sirin, Effect of hot dip galvanizing on the fatigue behavior of hot rolled and ion nitrided AISI 4340 steel, Int. J. Fatigue. 123 (2019) 1–9, https://doi.org/10.1016/j.ijfatigue.2019.01.001.
[10] M. Ozturk, F. Husem, I. Karademir, E. Maleki, A. Amanov, O. Unal, Fatigue crack growth rate of AISI 4140 low alloy steel treated via shot peening and plasma nitriding, Vacuum 207 (2023) 111552, https://doi.org/10.1016/j.vacuum.2022.111552.
[11] S.Y. Sirin, K. Sirin, E. Kaluc, Effect of the ion nitriding surface hardening process on fatigue behavior of AISI 4340 steel, Mater. Charact. 59 (2008) 351–358, https://doi.org/10.1016/j.matchar.2007.01.019.
[12] R. Mohammadzadeh, A. Akbari, M. Drouet, Microstructure and wear properties of AISI M2 tool steel on RF plasma nitriding at different N2-H2 gas compositions, Surf. Coatings Technol. 258 (2014) 566–573, https://doi.org/10.1016/j.surfcoat.2014.08.036.
[13] H. Kovacı, A.F. Yetim, O. Baran, A. Çelik, Fatigue crack growth analysis of plasma nitrided AISI 4140 low-alloy steel: Part 1-constant amplitude loading, Mater. Sci. Eng. a. 672 (2016) 257–264, https://doi.org/10.1016/j.msea.2016.07.002.
[14] D. Fernández-Valdés, A. Meneses-Amador, G.A. Rodríguez-Castro, I. Arzate-Vázquez, I. Campos-Silva, J.L. Nava-Sánchez, Standing contact fatigue behavior of nitrided AISI 316L steels, Surf. Coatings Technol. 377 (2019) 124871, https://doi.org/10.1016/j.surfcoat.2019.07.082.
[15] P. Landgraf, T. Bergelt, L.M. Rymer, C. Kipp, T. Grund, G. Bräuer, T. Lampke, Evolution of Microstructure and Hardness of the Nitrided Zone during Plasma Nitriding of High-Alloy Tool Steel, Metals (basel). 12 (2022) 1–22, https://doi.org/10.3390/met12050866.
[16] T. Bergelt, P. Landgraf, T. Grund, G. Bräuer, T. Lampke, Modelling of layer development and nitrogen distribution on different microstructures during plasma nitriding, Surf. Coatings Technol. 447 (2022), https://doi.org/10.1016/j.surfcoat.2022.128813.
[17] J.N. Jing, L.H. Dong, H.D. Wang, G. Jin, Influences of vacuum ion-nitriding on bending fatigue behaviors of 42CrMo4 steel: Experiment verification, numerical analysis and statistical approach, Int. J. Fatigue. 145 (2021) 106104, https://doi.org/10.1016/j.ijfatigue.2020.106104.
[18] S. Qin, L. Wang, L. Di, C. Zhang, M. Zhao, Effect of carburizing process on bending fatigue performance of notched parts of 18CrNiMo7-6 alloy steel, Eng. Fail. Anal. 147 (2023) 107161, https://doi.org/10.1016/j.engfailanal.2023.107161.
[19] M. Gabriela Galvão Camarinha, L. Contri Campanelli, M. Justino Ribeiro Barboza, L. Reis, A. Augusto Couto, D. Aparecida Pereira Reis, Fatigue behavior of notched and unnotched 7075-T6 aluminum alloy subjected to retrogression and re-aging (RRA) heat treatment and plasma nitriding, Theor. Appl. Fract. Mech. 127 (2023), https://doi.org/10.1016/j.tafmec.2023.104051.
[20] M.A. Terres, S. Ben Mohamed, H. Sidhom, Influence of ion nitriding on fatigue strength of low-alloy (42CrMo4) steel: Experimental characterization and predictive approach, Int. J. Fatigue. 32 (2010) 1795–1804, https://doi.org/10.1016/j.ijfatigue.2010.04.004.
[21] T. Connolley, P.E. Mchugh, M. Bruzzi, A review of deformation and fatigue of metals at small size scales, Fatigue Fract. Eng. Mater. Struct. 28 (2005) 1119–1152, https://doi.org/10.1111/j.1460-2695.2005.00951.x.
[22] S.O. Jeje, T. Marazani, M.B. Shongwe, Impact behavior of spark plasma sintered Ti–Al–Mo/TiN composites: a finite element analysis approach using Abaqus CAE, Beni-Suef Univ. J. Basic Appl. Sci. 13 (2024), https://doi.org/10.1186/s43088-024-00474-0.
[23] F. Yildiz, A.F. Yetim, A. Alsaran, A. Çelik, I. Kaymaz, Fretting fatigue properties of plasma nitrided AISI 316 L stainless steel: Experiments and finite element analysis, Tribol. Int. 44 (2011) 1979–1986, https://doi.org/10.1016/j.triboint.2011.08.011.
[24] F. Yildiz, A.F. Yetim, A. Alsaran, A. Çelik, I. Kaymaz, I. Efeoğlu, Plain and fretting fatigue behavior of Ti6Al4V alloy coated with TiAlN thin film, Tribol. Int. 66 (2013) 307–314, https://doi.org/10.1016/j.triboint.2013.06.006.
[25] J. Sawicki, P. Siedlaczek, A. Staszczyk, Finite-Element Analysis of Residual Stresses Generated Under Nitriding Process: a Three-Dimensional Model, Met. Sci. Heat Treat. 59 (2018) 799–804, https://doi.org/10.1007/s11041-018-0229-y.
[26] M.A. Khairul, S.M. Sapuan, F.M. Al-Oqla, E.S. Zainudin, Experimental investigation and numerical prediction for the fatigue life durability of austenitic stainless steel at room temperature, Eng. Solid Mech. 7 (2019) 121–130, https://doi.org/10.5267/j.esm.2019.4.001.
[27] H.E.R. Lake, "Peterson's stress concentration factors" Second edition, by W.D. Pilkey, Strain. 34 (1998) 71–71. 10.1111/j.1475-1305.1998.tb01083.x.
[28] A.H. Saleh, M.A. Nasser Ali, M.I. Ismail, A.N. Abood, The Radius Size Variation Effects on Fatigue Strength of AA6061-T6 and AA6061-O Alloys, IOP Conf. Ser, Mater. Sci. Eng. 518 (2019), https://doi.org/10.1088/1757-899X/518/3/032063.
[29] A.F. Yayla, R. Gecu, N. Solak, K. Kazmanli, M. Urgen, Measuring depth-dependent residual stresses in gaseous nitrided steels using indentation method, Mater. Res. Express. 11 (2024), https://doi.org/10.1088/2053-1591/ad719c.
[30] A. Alsaran, I. Kaymaz, Ç. Ayhan, F. Yetim, M. Karakan, A repair process for fatigue damage using plasma nitriding, Surf. Coatings Technol. 186 (2004) 333–338, https://doi.org/10.1016/j.surfcoat.2003.12.017.
[31] A. Çelik, A. Fatih Yetim, A. Alsaran, M. Karakan, Effect of magnetic treatment on fatigue life of AISI 4140 steel, Mater. Des. 26 (2005) 700–704, https://doi.org/10.1016/j.matdes.2004.09.003.
[32] Y.X. Zhao, Y. Zhang, H.W. He, Improved measurement on probabilistic fatigue limits/strengths by test data from staircase test method, Int. J. Fatigue. 94 (2017) 58–80, https://doi.org/10.1016/j.ijfatigue.2016.09.010.
[33] F. Yılan, H. Kovacı, Investigation of the Combined Effects of Stress Concentrations and Plasma Nitriding Parameters on the Fatigue Performance of AISI 4140 Low Alloy Steel, J. Mater. Eng. Perform. (2024), https://doi.org/10.1007/s11665-024-09424-4.
[34] R. Alkentar, F. Máté, T. Mankovits, Investigation of the Performance of Ti6Al4V Lattice Structures Designed for Biomedical Implants Using the Finite Element Method, Materials (basel). 15 (2022), https://doi.org/10.3390/ma15186335.
[35] B.C.E.S. Kurelo, G.B. De Souza, S.L.R. Da Silva, F.C. Serbena, C.E. Foerster, C. Alves, Plasma nitriding of HP13Cr supermartensitic stainless steel, Appl. Surf. Sci. 349 (2015) 403–414, https://doi.org/10.1016/j.apsusc.2015.04.202.

[36] M. Guagliano, L. Vergani, Effect of nitriding on low-cycle fatigue properties, Int. J. Fatigue. 19 (1997) 67–73, https://doi.org/10.1016/S0142-1123(96)00031-X.
[37] F.C. Barbieri, C. Otani, C.M. Lepienski, W.I. Urruchi, H.S. Maciel, G. Petraconi, Nanoindentation study of Ti6Al4V alloy nitrided by low intensity plasma jet process, Vacuum 67 (2002) 457–461, https://doi.org/10.1016/S0042-207X(02)00231-2.
[38] G.B. de Souza, C.E. Foerster, S.L.R. da Silva, F.C. Serbena, C.M. Lepienski, C.A. dos Santos, Hardness and elastic modulus of ion-nitrided titanium obtained by nanoindentation, Surf. Coatings Technol. 191 (2005) 76–82, https://doi.org/10.1016/j.surfcoat.2004.08.207.
[39] J. Fernández de Ara, E. Almandoz, J.F. Palacio, G.G. Fuentes, Simultaneous ageing and plasma nitriding of grade 300 maraging steel: How working pressure determines the effective nitrogen diffusion into narrow cavities, Surf. Coatings Technol. 317 (2017) 64–74, https://doi.org/10.1016/j.surfcoat.2017.02.060.
[40] D. Chaouch, S. Guessasma, A. Sadok, Finite Element simulation coupled to optimisation stochastic process to assess the effect of heat treatment on the mechanical properties of 42CrMo4 steel, Mater. Des. 34 (2012) 679–684, https://doi.org/10.1016/j.matdes.2011.05.026.
[41] Y. Li, Z. Liu, J. Luo, S. Zhang, J. Qiu, Y. He, Microstructure, mechanical and adhesive properties of CrN/CrTiAlSiN/WCrTiAlN multilayer coatings deposited on nitrided AISI 4140 steel, Mater. Charact. 147 (2019) 353–364, https://doi.org/10.1016/j.matchar.2018.11.017.
[42] A. Medina, J. Oseguera, H. Carreón, J. Ibarra, C. Aguilar, Analysis of microstructural parameters and quantification of phases in a plasma-nitrided AISI 4140 steel, Philos. Mag. Lett. 100 (2020) 452–460, https://doi.org/10.1080/09500839.2020.1799099.
[43] F.A.P. Fernandes, S.C. Heck, C.A. Picone, L.C. Casteletti, On the wear and corrosion of plasma nitrided AISI H13, Surf. Coatings Technol. 381 (2020) 125216, https://doi.org/10.1016/j.surfcoat.2019.125216.
[44] J. Valdés, J. Solis, R. Mercado, J. Oseguera, H. Carreón, C. Aguilar, A. Medina, Influence of plasma nitriding treatment on the micro-scale abrasive wear behavior of AISI 4140 steel, Mater. Lett. 324 (2022) 3–6, https://doi.org/10.1016/j.matlet.2022.132629.
[45] C. Allen, C.X. Li, T. Bell, Y. Sun, The effect of fretting on the fatigue behaviourof plasma nitrided stainless steels, Wear 254 (2003) 1106–1112, https://doi.org/10.1016/S0043-1648(03)00343-0.
[46] H. Kovacı, A.F. Yetim, A.Ç. Baran, Fatigue crack growth analysis of plasma nitrided AISI 4140 low-alloy steel: Part 2-Variable amplitude loading and load interactions, Mater. Sci. Eng. A. 672 (2016) 265–275, https://doi.org/10.1016/j.msea.2016.07.003.
[47] C. Ruset, S. Ciuca, E. Grigore, The influence of the sputtering process on the constitution of the compound layers obtained by plasma nitriding, Surf. Coatings Technol. 174–175 (2003) 1201–1205, https://doi.org/10.1016/S0257-8972(03)00589-9.
[48] H. Shen, L. Wang, Influence of temperature and duration on the nitriding behavior of 40Cr low alloy steel in mixture of NH3 and N2, Surf. Coatings Technol. 378 (2019) 124953, https://doi.org/10.1016/j.surfcoat.2019.124953.
[49] M.D. Conci, A.Ö.C. Bozzi, A.R. Franco, Effect of plasma nitriding potential on tribological behaviour of AISI D2 cold-worked tool steel, Wear 317 (2014) 188–193, https://doi.org/10.1016/j.wear.2014.05.012.
[50] M.S. Mahdipoor, D. Kevorkov, P. Jedrzejowski, M. Medraj, Water droplet erosion behaviour of gas nitrided Ti6Al4V, Surf. Coatings Technol. 292 (2016) 78–89, https://doi.org/10.1016/j.surfcoat.2016.03.032.
[51] W. Kong, V.M. Villapun, Y. Lu, L.N. Carter, M. Kuang, S. Cox, M.M. Attallah, The influence of thermal oxidation on the microstructure, fatigue properties, tribological and in vitro behaviour of laser powder bed fusion manufactured Ti-34 Nb-13Ta-5Zr-0.2O alloy, J. Alloys Compd. 929 (2022), https://doi.org/10.1016/j.jallcom.2022.167264.
[52] S. Bhuiyan, Y. Mutoh, Y. Miyashita, Y. Ostuka, Notch Effect on Fatigue Strength of Die Cast AM60 Magnesium Alloy, Asian Pacific Conf. Mater. Mech. (2009).
[53] Q. Bader, E.K. Njim, Effect of Stress Ratio and V Notch Shape on Fatigue Life in Steel Beam, Int. J. Sci. Eng. Res. 5 (2014) 1145–1154. 10.14299/ijser.2014.06.005.
[54] F. Ashrafizadeh, Influence of plasma and gas nitriding on fatigue resistance of plain carbon (Ck45) steel, Surf. Coatings Technol. 174–175 (2003) 1196–1200, https://doi.org/10.1016/S0257-8972(03)00460-2.
[55] S.M. Hassani-Gangaraj, A. Moridi, M. Guagliano, A. Ghidini, M. Boniardi, The effect of nitriding, severe shot peening and their combination on the fatigue behavior and micro-structure of a low-alloy steel, Int. J. Fatigue. 62 (2014) 67–76, https://doi.org/10.1016/j.ijfatigue.2013.04.017.
[56] C.M. Suh, J.K. Hwang, K.S. Son, H.K. Jang, Fatigue characteristics of nitrided SACM 645 according to the nitriding condition and notch, Mater. Sci. Eng. a. 392 (2005) 31–37, https://doi.org/10.1016/j.msea.2004.07.066.
[57] M. Akita, K. Tokaji, Effect of carburizing on notch fatigue behaviour in AISI 316 austenitic stainless steel, Surf. Coatings Technol. 200 (2006) 6073–6078, https://doi.org/10.1016/j.surfcoat.2005.09.018.
[58] Y. Peng, S. Zhang, Z. Liu, J. Gong, Notch fatigue behaviour of low-temperature gaseous carburised 316L austenitic stainless steel, Mater. Sci. Technol. (United Kingdom) 36 (2020) 1076–1082, https://doi.org/10.1080/02670836.2020.1753155.